

Ninja Codes: Neurally Generated Fiducial Markers for Stealthy 6-DoF Tracking

Yuichiro Takeuchi*

Yusuke Imoto†

Shunya Kato‡

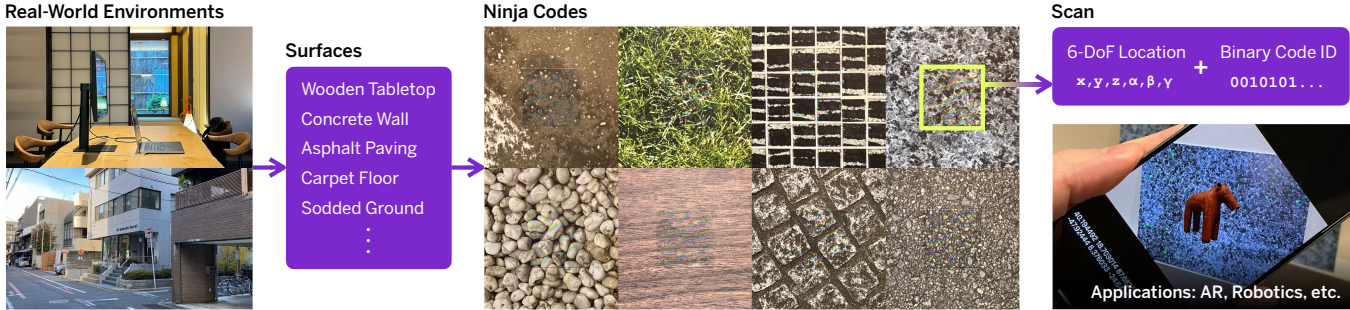


Figure 1: We present Ninja Codes, inconspicuous fiducial markers that can be made to blend into various real-world environments. An encoder network converts photos of surface textures into Ninja Codes, which can be printed out using standard color printers. Precise locations of Ninja Codes within scenes are obtained by capturing them with an RGB camera and passing the images through region/corner detector networks. The retrieved codes are processed by a decoder network to recover embedded messages, i.e., code IDs. Finally, the code locations/IDs are used to compute the position and pose of the capturing device.

Abstract

In this paper we describe Ninja Codes, neurally-generated fiducial markers that can be made to naturally blend into various real-world environments. An encoder network converts arbitrary images into Ninja Codes by applying visually modest alterations; the resulting codes, printed and pasted onto surfaces, can provide stealthy 6-DoF location tracking for a wide range of applications including augmented reality, robotics, motion-based user interfaces, etc. Ninja Codes can be printed using off-the-shelf color printers on regular printing paper, and can be detected using any device equipped with a modern RGB camera and capable of running inference. Using an end-to-end process inspired by prior work on deep steganography, we jointly train a series of network modules that perform the creation and detection of Ninja Codes. Through experiments, we demonstrate Ninja Codes' ability to provide reliable location tracking under common indoor lighting conditions, while successfully concealing themselves within diverse environmental textures. We expect Ninja Codes to offer particular value in scenarios where the conspicuous appearances of conventional fiducial markers make them undesirable for aesthetic and other reasons.

Keywords

Ninja Codes, fiducial markers, 6-DoF tracking, deep steganography, neural networks

1 Introduction

Precise, reliable location tracking is a foundation of numerous computing applications including augmented reality and robotics. While a wide range of solutions exist for this task, old-fashioned fiducial

markers – 2D graphical images that can be printed on paper and detected using computer vision – still retain broad appeal due to the combination of low cost, ease of deployment, and robust performance under varied environmental conditions. However, the typically eye-catching appearances of fiducial markers make their use unsuitable in some situations, especially those where aesthetic concerns carry weight. Hence, despite their widespread use in select environments such as research laboratories and warehouses, adoption in non-professional settings such as residential homes remains limited. Inconspicuous fiducial markers that are capable of seamlessly blending into environments can potentially introduce inexpensive, accurate location tracking to novel contexts.

In this paper we describe Ninja Codes (Figure 1), a new class of fiducial markers that deftly conceal themselves within various real-world environmental textures. Building on prior work in the field of deep steganography [2], where neural networks are used to surreptitiously encode binary messages within images, we train a neural network that turns arbitrary images into functional fiducial markers through subtle visual alterations. By creating Ninja Codes from photographs of wooden tabletops, tiled walls, asphalt paving, etc., discreet fiducial markers can be obtained that can be installed throughout environments in visually unobtrusive ways. Ninja Codes can be detected by a wide range of devices equipped with an RGB camera and capable of running inference – a category of devices which includes most modern smartphones – and can be printed on a variety of physical materials using commonly available equipment, e.g., an off-the-shelf color printer.

The Ninja Codes creation/detection pipeline comprises multiple neural network modules, including an encoder, decoder, and a pair of (i.e., region/corner) detector networks, which are trained jointly through an end-to-end process. Differentiable noise functions are applied at two different stages of the training process, to increase

*Wikitopia Research / Sony CSL Kyoto, email: yt@wikitopia.city

†Osaka University

‡Kyoto University

resistance to perturbations such as color shift owing to the printing method, specular reflection, camera noise, etc. We evaluated the performance of Ninja Codes through a series of experiments, and the results demonstrate their ability to both effectively conceal themselves from human detection, and provide reliable 6-DoF tracking under normal indoor lighting conditions.

The key contributions of this paper are as follows:

- Introduces Ninja Codes, a new class of fiducial markers that builds upon deep steganography techniques
- Reports experimental results demonstrating the codes' capabilities as a discreet location tracking solution
- Identifies outstanding issues and limitations, and maps out possible future improvements to the technology

A brief note on our terminology: In this paper, we use the term *location tracking* as a synonym for 6-DoF tracking of both position (x, y, z) and pose (α, β, γ) . Also, when we use the term *detection* with no qualifiers, we refer to the entire process of locating Ninja Codes within scenes, obtaining their corner coordinates, and retrieving the embedded code IDs – i.e., the combined operations of the region detector, corner detector, and decoder networks.

2 Related Work

2.1 Fiducial Markers

Modern variations of 2D fiducial markers first appeared in the early 1990s [11]. Since then, they have seen sustained use as a reliable and inexpensive location tracking technology, particularly in industrial and/or professional settings such as factories, warehouses, research laboratories, construction sites, etc. Examples of markers currently in wide use include ARTag [10], AprilTag [27], and ArUco [33], all of which encode relatively small amounts of data (typically 25 or 36 bits) in simple square images that can be printed using off-the-shelf printers. Apart from a small number of examples that employ non-rectilinear shapes [3, 20] or use non-grayscale color [8], most fiducial markers are monochrome and have grid-like appearances reminiscent of QR Codes but simpler due to smaller data capacities. (Whereas QR Codes are often used to encode variable-length strings such as website URLs or WiFi passwords, fiducial markers only need to contain short IDs to differentiate them from other markers. For example, a data capacity of 36 bits can represent 2^{36} , or more than 68 billion unique IDs.)

Most fiducial markers are detected using handcrafted algorithms, which locate markers within scenes, obtain their precise positions, and read out their IDs. However, within the past decade a string of work has explored the use of deep learning, either to detect existing markers like ArUco with better robustness to perturbations [17], or to develop entirely new fiducial markers that are both generated and detected by neural networks [13, 28]. A notable advantage of such neurally-generated markers is that through clever design of model architecture, training pipeline, etc., it is possible to develop markers with unique attributes that would be difficult, or at least considerably time-consuming, for humans to design by traditional means. DeepFormableTag [41] is one example of such work, where an end-to-end training process is used to generate markers that can retain effectiveness even when attached to non-planar surfaces.

Development of discreet or invisible fiducial markers that naturally blend into environments is a topic that has received relatively

modest attention, possibly due to the fact that fiducial markers are typically used in industrial or professional settings where aesthetic concerns are often deemed secondary. Proposed techniques include using infrared-absorbing ink [38] or fluorescent polymers [9] to create markers that are visible to specialized cameras but not to humans, and embedding hidden air pockets inside 3D printed objects that can be read out as markers by camera/projector combinations [22]. Outside of fiducial markers for location tracking, efforts have been made [39, 40, 42] to design aesthetically pleasing markers for data transmission, i.e., more attractive alternatives to QR Codes. (In recent years, it has also become common to see corporations introduce proprietary QR Code alternatives with distinctive aesthetic styles, e.g., Snapcode, Apple App Clip Code.)

Regular images can be appropriated as fiducial markers, in cases where only a small, predetermined set of images (with ample visual features) needs to serve as markers. Commercial augmented reality apps that use corporate logos or product packages to trigger effects are a prime example of this. (A classic, but still widely used method to implement such systems is to track feature vectors [25].) Such techniques can likely be used to create unobtrusive fiducial markers that naturally blend into real-world environments; however, they lack in scalability, a major strength of actual fiducial markers. For example, they cannot accommodate scenarios where a large number of mutually distinguishable markers must be placed throughout an environment – a necessary setup to offer reliable location tracking in any reasonably sized space.

2.2 Other Location Tracking Technologies

Outside of fiducial markers, there exists a number of alternative techniques to realize similar 6-DoF location tracking. Many techniques involve the use of external hardware such as WiFi basestations [1], ultrasound beacons [30], or infrared camera/illuminator combinations [29], and offer reliable, accurate tracking albeit with high costs of setup and operation which limit their utility outside of select professional use cases. There exist techniques that require no external hardware (or even markers), for example inertial sensing [4], SLAM [6], and so-called visual positioning systems (VPS) developed by corporations such as Google and Niantic Labs. Such wholly self-contained solutions may well be considered the *holy grail* of location tracking technologies, but fiducial markers still retain a significant edge in some scenarios – for example, SLAM/VPS tend to struggle in environments with repetitive or bland textures, and inertial sensing gives middling precision if not using high-end sensing devices which presently are unavailable on consumer devices like smartphones – and can often provide more robust tracking in use cases where the cost of marker installation is bearable.

A wide array of applications rely on precision location tracking. Augmented reality is a representative example, where the accuracy of location tracking has direct correlation to the breadth and quality of visual effects that can be implemented; advanced augmentation effects such as diminished reality [16, 26] and freeform transformations of environments [36] are only possible when precise 6-DoF tracking is available. Robotics is another domain where accurate location tracking is often critical. Research demos such as drone-based building construction [12] showcase the range of applications that can be realized with precision tracking in this area.

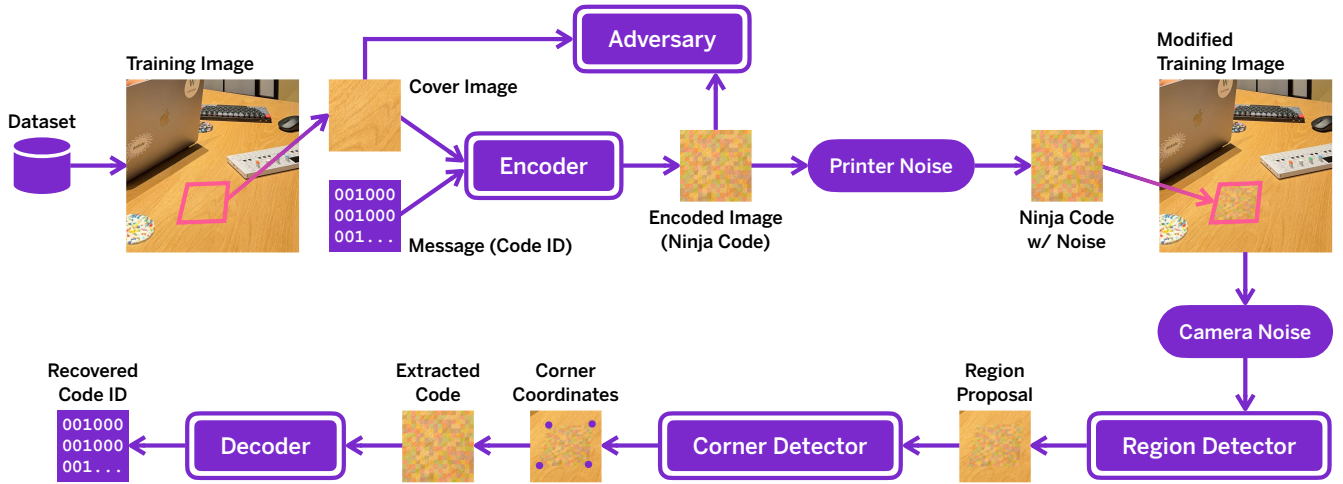


Figure 2: Ninja Codes end-to-end training architecture. A total of five modules are trained simultaneously: encoder, decoder, region detector, corner detector, and adversary. A series of differentiable noise functions are applied during the training process, to simulate perturbations that arise when printing and capturing the codes in real-world situations.

2.3 Deep Steganography

Steganography refers to the practice of surreptitiously embedding arbitrary messages within various media (most often images and video) – deep steganography [2] is its modern evolution that employs deep learning techniques. HiDDeN [44] and StegaStamp [37] are two notable examples of work in this area, both operating on a similar principle of jointly training encoder (which embeds data within images) and decoder (which recovers data from images) networks through an end-to-end process. Images encoded using these techniques show minimal signs of tampering, and are nearly indistinguishable to the human eye from unprocessed images. The field is still emerging but attracting growing interest from the research community, leading to numerous improvements and variations; for example, one proposed technique [19] allows data to be encoded in sub-images (small regions contained within larger images), opening up new use cases.

Our work on Ninja Codes borrows heavily from such precedents in deep steganography. Whereas prior work like HiDDeN exclusively concern themselves with the dual processes of encoding and decoding images, we attempt – taking inspiration from work on neural object detection [24, 31, 32] – to also enable encoded images, installed at unknown locations within environments in unknown numbers, to be accurately found and located down to their precise corner coordinates before retrieving the embedded messages (i.e., IDs). To our knowledge, our work represents the first example of neurally-generated fiducial markers that are made inconspicuous by using the principles of deep steganography.

3 Ninja Codes

3.1 Overview

Figure 2 illustrates the end-to-end process used to simultaneously train the multiple network modules comprising the Ninja Codes creation/detection pipeline.

For each image sampled from the training dataset (our training images have a uniform resolution of 1024×1024 ; details regarding dataset preparation will be given later), up to four square patches of random sizes are cut out at random locations. The patches are then warped (each vertex is shifted randomly in both x and y directions, with maximum amplitude set to 15% of the patch’s edge length) and randomly rotated to form convex quadrilaterals. The quadrilaterals are extracted from the training image, then geometrically rectified and resized into 256×256 square images – borrowing terminology from steganography research, we call these *cover images*.

Next, each cover image, along with a randomly generated 36-bit binary message (code ID), is given to the encoder which outputs an encoded image, i.e., Ninja Code. After applying a series of noise functions intended to simulate perturbations owing to the printing method/material (e.g., color shift), the Ninja Codes are re-warped and pasted back onto the training images that they had originally been cut out from; the resulting images mimic real-world scenes in which Ninja Codes have been attached onto various environmental surfaces. A second round of noise functions is applied to these images, this time with the intention to simulate perturbations arising from the camera capture process (e.g., optical blur). The images are then resized to 300×300 , and given as input to the region detector which locates square regions within images that are deemed likely to contain Ninja Codes. The results are then refined by the corner detector, to obtain the codes’ corner coordinates.

The detected Ninja Codes are geometrically rectified, scaled to 256×256 , and given to the decoder to retrieve their IDs. Provided that both the world coordinates and physical dimensions of the individual Ninja Codes are known, the 6-DoF position of the capturing device (e.g., smartphone camera) can be computed using a least squares approach. (Many computer vision packages such as OpenCV provide functions that perform this computation; we will omit technical details here, since they are outside the scope of this paper and the technique is well established at this point.)

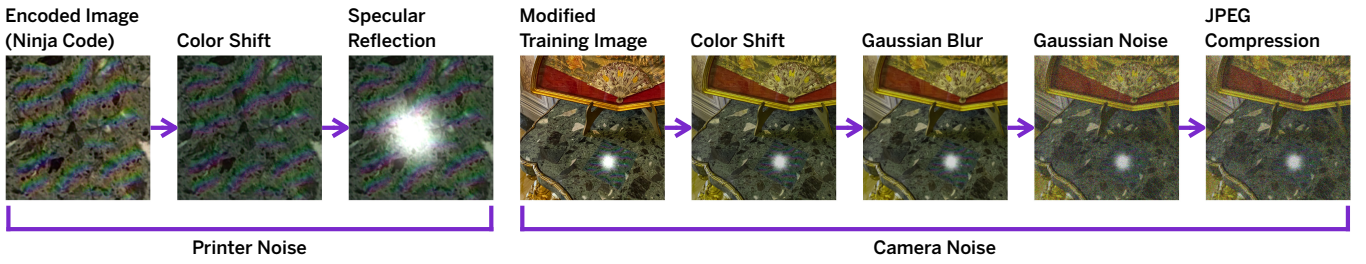


Figure 3: Noise functions to simulate perturbations. Perturbations owing to the printing method/material are simulated using color shift and synthetic specular reflection. Perturbations owing to camera capture are simulated using color shift, Gaussian blur, Gaussian noise, and JPEG compression.

3.2 Models

Below are descriptions of the five neural network models shown in Figure 2, which we train jointly in an end-to-end manner.

3.2.1 Encoder. The encoder takes an RGB cover image and a 36-bit binary message (i.e., code ID) as input. The message is preprocessed using a linear transformation block to produce a tensor with the same dimensions as the cover image (256×256 , 3 channels), which is then concatenated with the cover image at the channel dimension. The resulting 6-channel tensor is passed on to a U-Net [34], whose output is an encoded Ninja Code.

3.2.2 Region Detector. The region detector is a single-class object detector based on the SSD [24] architecture, which takes a 300×300 image as input and outputs a series of square regions, each deemed to contain a Ninja Code with high probability. While most modern SSD implementations employ a ResNet [15] backbone, we use VGG [35] instead as we have found it to lead to faster convergence with no noticeable negative impact on performance in our specific case. While SSD and other neural object detectors typically use variable-shaped anchors, here we only use square anchors since we are only interested in locating Ninja Codes which have a square shape (and roughly square, even when seen from angles); this has the effect of reducing the number of parameters, making training feasible on relatively inexpensive GPUs.

3.2.3 Corner Detector. The corner detector is another U-Net (with fewer layers compared to the one used in the encoder), followed by a series of fully-connected layers. It takes the output of the region detector (i.e., region proposals), and directly computes four sets of x, y coordinates (i.e., the four corner points of the Ninja Code) for each proposed region. Alternatively, the final layers of the model can be replaced with a convolution to output a heatmap [5]. While heatmaps appear to be the more common choice in state-of-the-art keypoint estimation models, we opt for direct regression here, as we found it to yield better results in edge cases where Ninja Codes partially lie outside of the camera frame.

3.2.4 Decoder. The decoder is a simple sequence of convolutional blocks, followed by a pair of fully-connected layers. Unlike some prior work [37] on deep steganography, we do not include a spatial transformer [18] to increase robustness to geometric perturbations. Our rationale here is that, if the region and corner detectors are performing to expected levels the input to the decoder should have

minimal geometric perturbations to begin with; hence, introducing additional mechanisms here will make training more expensive for likely little material gain.

3.2.5 Adversary. The adversary is also a simple series of convolutional blocks, followed by averaging pooling and a fully-connected layer. It takes a 256×256 RGB image as input, and outputs its belief (in the form of logit scores) on whether the input was a Ninja Code or the original cover image.

3.3 Noise

Figure 3 illustrates the noise functions that are applied at two separate stages during the training process.

3.3.1 Printer Noise. The first set of noise functions is designed to simulate perturbations arising from the printing method/material, and is applied to all Ninja Codes immediately after they have been generated by the encoder. We perform a color shift where the hue, brightness, contrast, and saturation of the Ninja Codes are adjusted randomly within predefined ranges (hue: ± 0.1 , brightness: $\pm 10\%$, contrast and saturation: $\pm 15\%$). We also render a synthetic specular reflection of randomized size, shape, and intensity using a series of differentiable tensor operations, which is overlaid on each code; this function was informed by the observation that many brands of regular printing paper show moderate degrees of glossiness which can disrupt detection.

3.3.2 Camera Noise. The second set of noise functions is applied to images passed on to the region detector (i.e., images intended to mimic real-world scenes with Ninja Codes attached to surfaces), to simulate perturbations resulting from the camera capture process. We again apply a randomized color shift to the images (details are identical to the earlier operation), followed by Gaussian blur (with kernel size randomly chosen from 1, 3, 5, and 7 pixels), Gaussian noise (with σ sampled from uniform distribution $[0, 0.2]$), and JPEG compression (with random Q value). Unlike [37], we do not apply any geometric transformations as part of the noise functions. This is because the method by which we extract cover images from each training image (discussed in section 3.1) already ensures robustness to both perspective warp and rotation, and adding such operations here would be redundant.

3.3.3 Adapting Noise Functions. Note that our noise functions have been designed with a specific range of use cases in mind; in particular, we assume that Ninja Codes will be printed using standard

color printers on regular paper, and will be captured by common RGB cameras (such as those on smartphones) under unexceptional lighting conditions. Accommodating scenarios outside of this assumption will likely require a modified set of noise functions. For example, although Ninja Codes can theoretically be embedded into surface textures of full-color 3D printed objects, the training process will need to be updated to reflect the different, typically more limited color space afforded by 3D printers.

3.4 Loss Function

We jointly train the encoder, decoder, and region/corner detector networks by minimizing loss function L_{total} , which is a weighted sum of the following losses.

The **Image Loss** (L_i) is a quantification of the visual disparity between Ninja Codes and the original cover images. The loss can be further decomposed as $L_i = L_{pixel} + L_{chroma} + 0.01 * L_{lpips}$. Here, L_{pixel} is the pixel MSE between Ninja Codes and cover images in YUV color space, each channel weighted separately to account for sensitivity characteristics of human vision. L_{chroma} is a smooth L1 loss intended to ensure that chroma (UV) deviations from cover images remain balanced, i.e., it tries to prevent Ninja Codes from becoming overly reddish, bluish, etc. L_{lpips} is the LPIPS learned perceptual similarity metric, first described in [43].

The **Regression Loss** (L_r) and **Classification Loss** (L_c) denote the levels of positional error and content classification error, both pertaining to region detector output. As our region detector is SSD-based, following [24] we take the smooth L1 loss for the former and cross entropy loss for the latter.

The **Keypoint Loss** (L_k) is the degree of error in corner detector output; it measures the difference (as MSE) between predicted corner coordinates and the corresponding ground truth values.

The **Message Loss** (L_m) is the degree of error in decoder output, i.e., the difference between retrieved and originally-assigned IDs of Ninja Codes. Again we use MSE to compute this value.

The **Adversary Loss** (L_a) is the degree to which the adversary could successfully distinguish Ninja Codes from unencoded images, obtained by giving Ninja Codes to the adversary, and calculating the cross entropy loss using its output logits.

To summarize, the total loss is expressed as follows, with w_i , w_r , w_c , w_k , w_m , w_a denoting weights for the respective losses.

$$L_{total} = w_i L_i + w_r L_r + w_c L_c + w_k L_k + w_m L_m + w_a L_a$$

Note that although L_{total} includes the adversary loss, this loss is not used to train the adversary itself – it is instead trained separately from the other four models, using the reverse of L_a (i.e., the extent to which the adversary *failed* to distinguish between Ninja Codes and unencoded images) as the loss function.

3.5 Training

3.5.1 Setup. We performed training on an Ubuntu Linux workstation equipped with dual NVIDIA RTX 3090 GPUs. Training the full pipeline illustrated in Figure 2 takes approximately 45 minutes per epoch on this machine. Software was written in Python using the Pytorch library. For all training we used the Adam [21] optimizer,

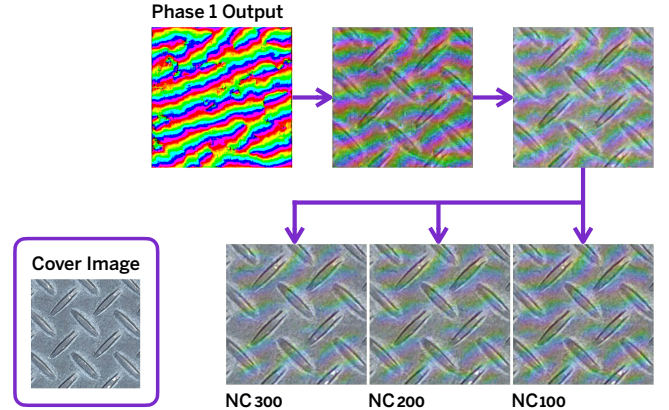


Figure 4: We employ a two-phase training process. After the first phase, the encoder will have learned to produce brightly-colored Ninja Codes (top left). After the second phase, the encoder will produce Ninja Codes closer to the cover image albeit with residual visual artifacts (bottom). Artifact saliency can be controlled by adjusting hyperparameters.

with initial learning rate set to $1.0e^{-5}$, weight decay set to zero, and $(\beta_1, \beta_2, \epsilon)$ set to $(0.9, 0.999, 1.0e^{-8})$, respectively.

3.5.2 Dataset. The training dataset contains 48,000 images in total, consisting of 43,300 images from the Common Objects in Context (COCO) 2014 dataset [23] (a general-purpose dataset containing images of varied content), and 4,700 images from DTD (Describable Textures Dataset) [7] which exclusively contains texture images. Each image is resized and cropped to a uniform size of 1024×1024 . The validation dataset contains 9,600 images, consisting of 8,660 images from COCO and 940 images from DTD.

3.5.3 Training (Phase 1). Though it is possible to perform training in a single pass, we found that splitting the process into two separate phases leads to more reliable convergence and predictable results. In the first phase, we ignore image loss, message loss, and adversary loss (i.e., we set their relative weights to zero), and focus solely on improving region and corner detection performance (w_r , w_c , w_k are set to 1.0, 1.0, and $1.0e^5$, respectively). We train for 20 epochs, after which the encoder will output conspicuous Ninja Codes marked by colorful stripes, as shown in Figure 4 (top left). At this point, the codes can already be robustly detected by the region and corner detectors. The visual pattern of the stripes is an emergent feature, and manifests differently each time training is conducted.

3.5.4 Training (Phase 2). In the second phase, we move on to training the entire pipeline. We train for 60 epochs in total; weights are initially set to $w_i = w_r = w_c = 1.0$, $w_k = 1.0e^5$, $w_m = 10.0$, and $w_a = 0.001$, and w_i is progressively increased to 100.0 over the first 30 epochs. For the remaining 30 epochs, for testing purposes we performed training in three separate sessions, with w_i set to 100.0, 200.0, and 300.0, respectively. In the end we obtained three sets of modules, each trained for 60 epochs (80 if the first phase is included), which we hereafter refer to as NC_{100} , NC_{200} , and NC_{300} . Over the course of training, the encoder will learn to generate Ninja Codes that, while retaining some characteristic details of the earlier codes as

visual artifacts, show increasing resemblance to the cover images (Figure 4, bottom). Expectedly, setting w_i to higher values leads to decreased levels of visual artifacts. However, unlike with state-of-the-art deep steganography techniques, so far we have only been able to suppress artifacts — without catastrophic drops in detection performance — to levels where they are still noticeable to human inspection. Further suppression is likely possible through improvements in model architecture, etc., but a degree of saliency is perhaps necessitated by the requirement that Ninja Codes must be robustly discoverable within scenes.

Since we train all models jointly, network modules can only be expected to work with other modules that have been co-trained in the same session. However, it may be convenient if we can train multiple encoders using a variety of parameters (e.g., different w_i values) to accommodate different use cases — for example, pursue greater artifact suppression if the codes are to be pasted onto bland, light-colored surfaces — and train a single set of detector/decoder modules that can handle codes created using any of the encoders. To test if this works in practice, we took the trained modules from NC_{100} and performed 30 additional epochs of fine-tuning, to make them capable of detecting codes generated using all three (NC_{100} , NC_{200} , NC_{300}) encoders.

4 Evaluation

We conducted a series of experiments to evaluate the performance of Ninja Codes.

4.1 Code Detection Performance Test

First, to test the accuracy of region/corner detection and message (code ID) retrieval, i.e., the entire detection pipeline, we prepared 25 high-resolution images of common environmental textures such as wood, marble, asphalt, etc., and converted the central portion of each image into a Ninja Code using the NC_{100} , NC_{200} , and NC_{300} encoders (Figure 5, top). We displayed each image on a 22-inch LG UltraFine 5K monitor (scaled so that the Ninja Code was shown at a size of 8.5×8.5cm on the screen), and took a series of photographs from eight camera positions (Figure 5, bottom) using a custom application we built for the Apple iPhone 15 Pro. All photos were shot in 1080×1080 resolution, and at each of the eight positions, camera orientation was adjusted so that the center of the LG monitor screen coincided with the center of the captured photo. All photos were automatically passed on to the trained detector/decoder modules (running locally on the iPhone), to locate the codes, obtain their corner coordinates, and retrieve their IDs. The test was conducted in a well-lit indoor room.

For this first test, we focused on measuring the average corner error (in pixels) and the drop rate (percentage of failed detections, i.e., false negatives). From each of the eight camera positions, the app took five photos at one-second intervals. The failed detection rate was measured by counting the number of photos in which the modules either failed to find the Ninja Code, or failed to correctly retrieve the 36-bit code ID in its entirety. The corner error was measured using the first photo in which a Ninja Code was successfully detected with the code ID intact; the predicted coordinate values were compared with ground truth values obtained beforehand for each of the eight camera positions. In cases where the app failed to

detect Ninja Codes in all five photos, we registered the drop rate as 100% and let the app continue to take photos until a successful detection occurred, from which we measured the corner error.

We conducted the test three separate times, for each of the three sets of trained modules: NC_{100} , NC_{200} , and NC_{300} . In addition, we conducted the same test three more times, this time using the fine-tuned detector/decoder modules (discussed at the end of section 3.5) which were trained to handle codes generated using any of the three encoders (hereafter abbreviated as FT modules). Lastly, for comparison we conducted the same test with ArUco markers used in place of Ninja Codes.

Table 1 shows the results of this first test. The average corner error for Ninja Codes hovers around one pixel, which is larger than that of ArUco but still quite small in absolute terms. Surprisingly, we did not see significant differences in error values between the eight

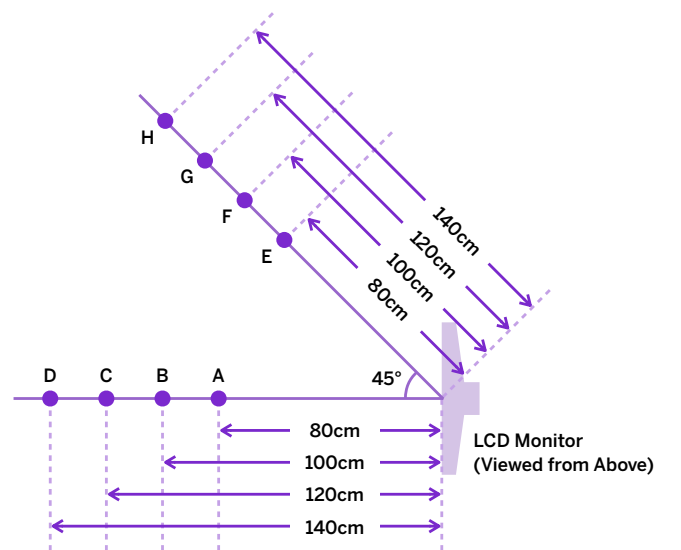
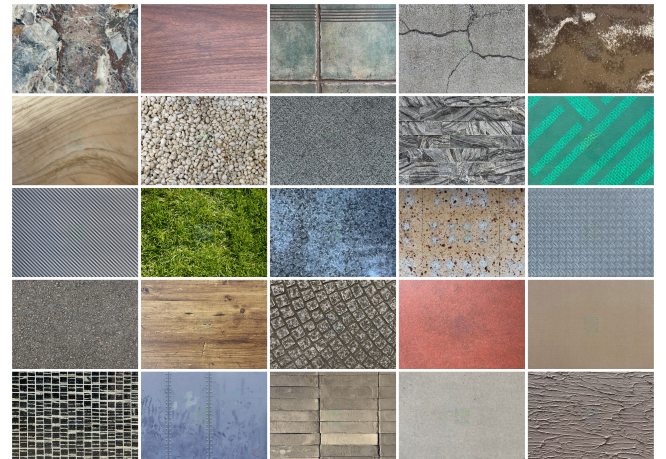


Figure 5: The 25 digital images used to evaluate code detection performance, each with a single Ninja Code (here, generated using the NC_{300} encoder) placed at the center (top). The eight camera positions (bottom).

Table 1: Code Detection Performance Results

	Corner Error (px)	Drop Rate (%)
NC_{100}	0.994	3.20
NC_{200}	1.057	7.30
NC_{300}	1.145	11.10
$NC_{100} + FT$	0.958	3.50
$NC_{200} + FT$	1.042	5.90
$NC_{300} + FT$	1.220	12.80
ArUco	0.586	0.00

camera positions; the average error appeared to stay around one pixel, regardless of the distance and angle from which the photo was taken. Also, the fine-tuned *FT* modules yielded results similar to those for dedicated modules, suggesting the feasibility of preparing a suite of Ninja Codes (each catering to different usage scenarios) which can be detected by a single set of detector/decoder modules. (Note: Although all photos were shot in 1080×1080 resolution, the region detector accepts 300×300 images and thus performs a scaling operation before processing. Values in Table 1 are reported in that scale, and should be interpreted accordingly. To ensure fair comparison, ArUco markers were also detected from similarly scaled down images.)

Concerningly, the results also show high rates of failed detections, especially for NC_{300} which was trained with the highest w_i value. We noticed that failed detections were background-specific, i.e., they did not occur at similar rates for all background textures but were instead concentrated around those with seemingly high visual contrast. For each image, we quantified its contrast intensity using local RMS (standard deviation of pixel YUV values, computed at small patches throughout the image and then averaged); the two images with the highest local RMS — the grass texture image in the third row, second column in Figure 5 (top), and the tile image at the bottom left corner — coincided with those that produced the most failed detections. (If we omit these two images from our analysis, the drop rate decreases to 1.30% for NC_{100} , 4.67% for NC_{200} , and 8.15% for NC_{300} .) This fact may possibly be used to caution users when they attempt to create Ninja Codes from cover images with overly high visual contrast.

Furthermore, we noticed that a number of failed detections were caused by faulty retrieval of code ID, i.e., the Ninja Code had been successfully located but the decoder failed to recover the embedded message in full. This suggests that the drop rate may be alleviated by employing error correction, using part of the 36-bit message as check symbols. To test this, we created an alternative set of NC_{300} codes where 12 of the 36 bits were designated as check symbols, and implemented Reed-Solomon error correction to repair corrupt bits (if any) after decoding. While this has the effect of reducing the number of unique IDs that can be represented — to approximately 16.8 million from 68.7 billion — subsequent testing (conducted in the same manner as the earlier tests) yielded a significant decrease in drop rate, to 6.00 from 11.10.

Overall, the results show that Ninja Codes can be detected with impressive accuracy, with a few caveats: the tendency to struggle with high-contrast background textures, and the possible need to

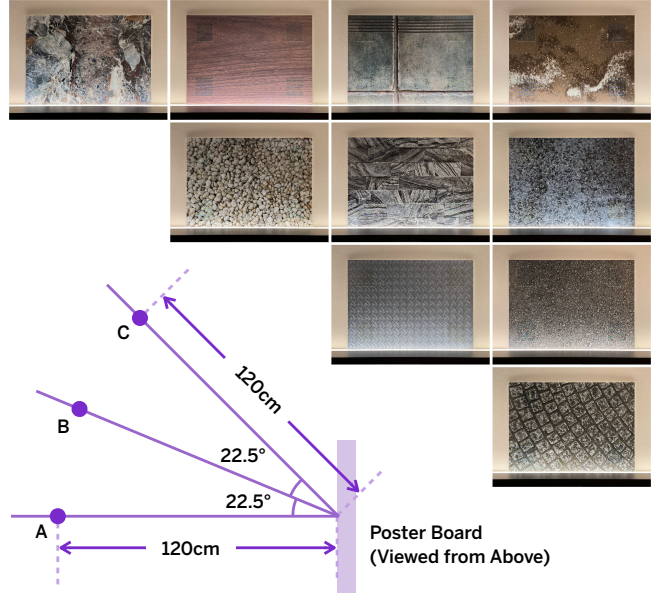


Figure 6: Poster boards used to evaluate 6-DoF tracking performance, with four Ninja Codes (generated using the NC_{200} encoder) placed at the corners (top). The three camera positions (bottom).

employ error correction (hence reducing data capacity) when using encoders with strong artifact suppression.

4.2 6-DoF Tracking Performance Test

Next, we prepared ten A2 size (59.4×42.0 cm) poster boards (Figure 6, top), each showing a texture image picked out from the 25 images used in the previous test. (Out of the 25 images, we first excluded the two with the highest visual contrast, and handpicked ten from the rest.) We attached four 8.5×8.5 cm Ninja Codes (generated using the mid-level NC_{200} encoder) to the four corners of the boards, and for each board, shot a series of ten photographs from each of three camera positions (Figure 6, bottom). For each of the three positions, camera orientation was adjusted so that the center of the poster board coincided with the center of the captured photo. In addition, for comparison we conducted the same test with ArUco markers used in place of Ninja Codes. Again, all photos were shot using our custom application on an iPhone 15 Pro, in 1080×1080 resolution. Both the poster boards and the Ninja Codes were printed using an HP DesignJet Z9 large-format printer. The test was conducted in a well-lit indoor environment.

For this test, in addition to detecting the codes and recovering their IDs, we used the code location/ID combinations to calculate the 6-DoF position/pose of the iPhone camera. (All processing was done locally on the iPhone 15 Pro.) Here, our goal was to evaluate how much the corner detection accuracy of Ninja Codes — which we found to be slightly lower compared to that of ArUco — affects their 6-DoF tracking performance. In addition, we aimed to see if the difference in materials (Ninja Codes were printed on paper this time) leads to any negative effects, and if the modules are capable of reliably tracking multiple Ninja Codes simultaneously.

Table 2 shows the results. We can see that Ninja Codes, while not quite matching the performance of ArUco, yields centimeter-level (position) and nearly single-degree (pose) accuracy which should be sufficient for a broad range of use cases. We did not observe issues regarding multi-code detection; nor did we observe adverse effects attributable to the printing method or material, demonstrating the effectiveness of our printer noise functions.

Table 2: 6-DoF Tracking Performance Results

	Position Error (cm)	Pose Error (degrees)
NC_{200}	2.988	1.084
ArUco	2.121	0.854

4.3 Visual Conspicuity Test

To evaluate how well Ninja Codes are able to conceal themselves from human detection, we conducted a software-based test using a custom application we built for the Microsoft Surface Pro 7 touch-screen laptop. The application shows a full-screen rendering of a texture image (randomly sampled from DTD), onto which a single Ninja Code is overlaid with randomized size and location. Tapping on the Ninja Code triggers the software to record the time passed since the image was displayed; tapping anywhere else on the screen does nothing. We recruited nine test subjects in a university setting (all male undergraduate/graduate students, average age: 23.4), and measured the time required for them to locate Ninja Codes on the software. For comparison, we prepared another version of the app where ArUco markers were overlaid instead of Ninja Codes. Each subject was shown 25 code-overlaid images for both versions of the app (i.e., 50 images total per subject), and for each image was asked to locate and tap on the code as quickly as possible. Due to scheduling and logistical issues, Ninja Codes in this test were created using a prototype version of the encoder which output codes with stronger visual artifacts compared to the newer (i.e., NC_{100} , NC_{200} , NC_{300}) encoders (Figure 7).

Figure 8 shows the results. Locating Ninja Codes took significantly more time for the test subjects, compared to ArUco markers which were generally detected promptly. Detection time was also highly variable for Ninja Codes (in one exceptional case, a subject needed more than 38 seconds to locate a Ninja Code); background images with high visual contrast seemed to cause particular trouble for the subjects — interestingly, the same types of images that led to high rates of failed detections in the first test.

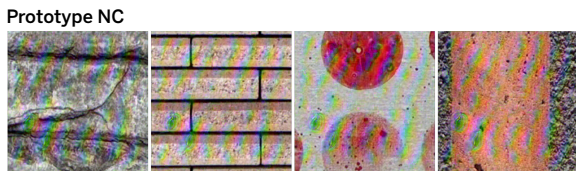


Figure 7: Prototype Ninja Codes used to evaluate visual conspicuity, which exhibit stronger visual artifacts compared to the newer encoders.

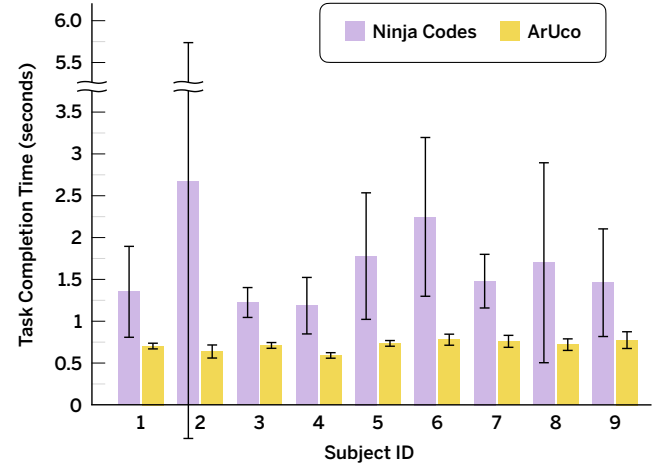


Figure 8: Average time from image display to code detection for Ninja Codes and ArUco (in seconds). Error bars represent 95% confidence interval.

4.4 Informal Observations

In addition to the above quantitative evaluations, to gain insights regarding how Ninja Codes may perform in real-world usage scenarios, we extended our custom iPhone app giving it a rudimentary augmented reality function (the app overlays simple graphics on top of Ninja Codes, corresponding to their IDs) and informally used it in an indoor environment where multiple Ninja Codes had been installed beforehand (Figure 9, left and top). Our aim here was to see if we encounter any issues or peculiarities which had not been revealed through the earlier experiments. All codes were generated

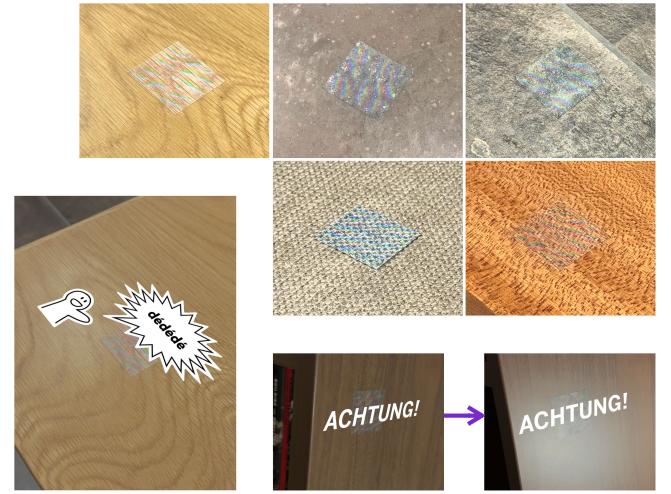


Figure 9: Ninja Codes (top) and a simple augmented reality app (left) used for informal observations. We noticed that material differences make the codes more noticeable compared to paper-on-paper installation. The codes exhibit reasonable robustness to changes in lighting conditions (bottom right), including occlusions caused by specular reflection.

using the NC_{300} encoder, and printed using a Fujifilm Multifunction printer as 4.25×4.25 cm squares at a local convenience store.

As a result, our experiences largely conformed to prior expectations. One issue we found, however, was that material differences between the Ninja Codes (printed on regular printing paper) and background surfaces often made the codes easily noticeable, especially for surfaces with three-dimensional textures such as textiles. Regarding detection performance, Ninja Codes could be robustly detected under a wide range of lighting conditions, including cases where the codes were partially occluded due to specular reflection (Figure 9, bottom) — suggesting that binary data is encoded within Ninja Codes in a spatially redundant manner, as per our intention in designing the noise functions. In addition, we noticed that detection performance tends to deteriorate less for underilluminated situations than overilluminated ones. Though we suspect that this has more to do with the specifics of iPhone’s autoexposure algorithm (we noticed a slight tendency to overexposure) than Ninja Codes per se, a small change in the range of brightness shift in the camera noise functions may suffice as a quick remedy.

5 Discussion

Through experiments, we have demonstrated the potential of Ninja Codes as a promising new class of fiducial markers that can bring reliable, inexpensive location tracking to new contexts, including those where aesthetic concerns take priority. We believe the codes to have potential uses in residential homes, retail stores, museums, public plazas/streets, and many other contexts — but the technology needs substantial refinement before real-world deployment.

Below, we list several outstanding issues and limitations (along with possible countermeasures) regarding our current implementation of Ninja Codes, and also discuss some avenues for extension and future development.

5.1 Limitations

5.1.1 Visual Artifacts. Modern steganography techniques produce encoded images with minimal discernible visual artifacts; in contrast, although Ninja Codes hide themselves well from human detection (as we have shown in section 4.3), artifacts are still clearly visible upon inspection, and become especially noticeable when codes are created from plain or light-colored cover images (Figure 10). While further artifact suppression should be possible through architectural refinements, preparation of dedicated datasets that align more closely with the range of anticipated cover images, etc., the need for robust detection under diverse environmental conditions will likely impose a limit on artifact minimization.

Since under our two-phase training scheme, the general characteristics of artifacts are carried over from the visual patterns that arise in the first phase (Figure 4), an alternative strategy may be to pursue aesthetic control of these emergent patterns by introducing new loss functions, i.e., to accept the presence of modest artifacts but ensure they will be aesthetically unobjectionable.

5.1.2 Maximum Range. In our current implementation, the region detector accepts 300×300 images as input. At this resolution, Ninja Codes with smaller dimensions, or those located far away from the camera, fail to retain enough visual features for them to be robustly detected. Under the experimental setup described in section 4.1, the

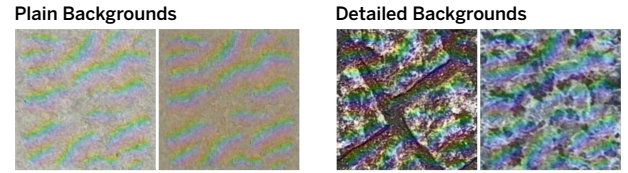


Figure 10: Artifacts register more strongly for plain or light-colored background textures.

maximum distance from which our modules could reliably detect the 8.5×8.5 cm Ninja Codes was approximately 160cm.

This is a commonly encountered issue with neural object detection, and has a rather straightforward solution; we can redesign the region detector to accept higher-resolution images. However, this will come with the byproduct of increased model size, hence slower training and inference. For reference, our current detector/decoder modules have a combined inference time of around 30 milliseconds on the iPhone 15 Pro, leaving ample time for additional processing (e.g., graphics rendering) while maintaining usable frame rates.

5.1.3 Privacy. Location data is closely tied to privacy issues, and in many jurisdictions is considered sensitive personal data subject to protection. As a new technology that potentially expands the range of contexts in which location tracking is used, the development of Ninja Codes must proceed in tandem with development of effective privacy protection measures. To give an example, if a person takes a photo in an environment where Ninja Codes are installed and uploads it to the Internet, an attacker may be able to extract precise location information even if the file had been stripped of relevant metadata. A possible defense — albeit an incomplete one — may be mounted against such attacks, by exploiting the fact that each time we train the full Ninja Codes pipeline, mutually non-interoperable sets of modules are newly generated; hence we can create “private” versions of Ninja Codes, and only distribute their detector/decoder modules to trusted parties.

5.2 Extensions and Future Work

5.2.1 Reverse Encoder. One interesting finding we made through our experimentations is that a standard U-Net model can be trained

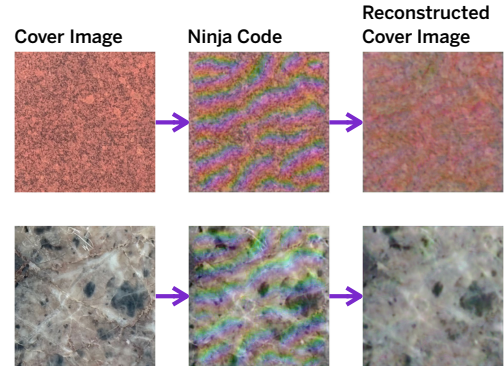


Figure 11: A reverse encoder that takes a Ninja Code as input and attempts to reconstruct the cover image.

to function as a *reverse encoder*, which takes a Ninja Code as input and attempts to reconstruct the original cover image (Figure 11). While further improvements are needed to curb the loss of visual details, this may be useful, for example, in augmented reality applications where we wish to remove hints of Ninja Codes in the final augmented scene, such as when using them in a film production setting as anchors to position CGI elements in space.

The reverse encoder may also serve as another line of defense against the aforementioned privacy issue, by enabling Ninja Codes to be automatically obscured in photographs to prevent surreptitious extraction of location information.

5.2.2 Color Calibration. Performing color calibration is critical to minimize visual discontinuities between Ninja Codes and their background surfaces (Figure 12, left). While specialized hardware and techniques exist [14] for such purposes and are widely used in professional settings, deploying such sophisticated solutions in real-life scenarios is often impractical. For the informal observation session described in section 4.4, we have built and used a simple tool (Figure 12, right) that assists calibration by capturing photos under controlled LED lighting. We plan to further develop this tool, improving usability and also enabling it to capture various material properties such as reflectance functions.

5.2.3 Materiality. Our current implementation expects that Ninja Codes will primarily be printed on paper. However, the underlying concept is theoretically adaptable to other types of media whose fabrication processes can be digitally controlled, such as textiles and 3D printed objects. Expanding materiality to better reflect the physical heterogeneity of the real world would give us a broader set of options for concealing Ninja Codes within environments (as discussed in section 4.4, material differences can make Ninja Codes easily noticeable even with sound color correction); we view this as an important future direction for this work.

In practice, adapting the technology to accommodate new media can require nontrivial modifications to model architecture, training pipeline, etc. However, in the restricted case of extending to other 2D materials — or 2D surfaces of 3D objects — adequate results may

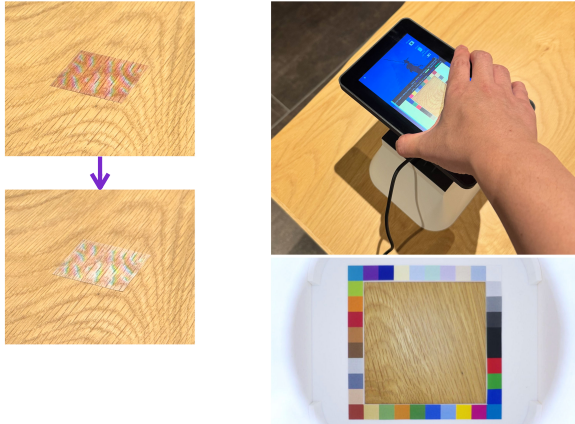


Figure 12: Faulty color calibration results in color discontinuity (left). A photographic tool that captures surface textures under controlled LED lighting (right).

be achievable by simply updating noise functions to handle color space differences (as discussed in section 3.3).

6 Conclusion

In this paper we described Ninja Codes, neurally-generated fiducial markers that blend naturally into real-world environments. While the generated codes still exhibit some noticeable artifacts, as shown through our experiments they effectively conceal themselves from human attention while providing accurate 6-DoF location tracking. We believe that the inconspicuous nature of Ninja Codes can make their use attractive in a wide range of domestic, commercial, and outdoor settings where conventional fiducial markers have so far failed to gain widespread use. With further refinements, we foresee the technology as providing the necessary foundation for various applications that rely on precision location tracking to make their ways into new contexts. Our future work will focus on improving detection performance (to better match those of existing fiducial markers), tackling aesthetic deficiencies including artifact production, exploring new materiality options, and developing techniques and mechanisms for privacy protection.

References

- [1] Bahl, V. and Padmanabhan, V. RADAR: An In-Building RF-based User Location and Tracking System. In Proc. of IEEE INFOCOM 2000, 775–784.
- [2] Baluja, S. Hiding Images in Plain Sight: Deep Steganography. In Proc. of NeurIPS 2017, 2066–2076.
- [3] Bergamasco, F., Albarelli, A., Rodolà, E., Torsello, A. RUNE-Tag: A High Accuracy Fiducial Marker with Strong Occlusion Resilience. In Proc. of CVPR 2011, 113–120.
- [4] Brossard, M., Barrau, A., Bonnabel, S. AI-IMU Dead-Reckoning. IEEE Trans. on Intelligent Vehicles 5 (4), 585–595. 2019.
- [5] Bulat, A., and Tzimiropoulos, G. Human Pose Estimation via Convolutional Part Heatmap Regression. In Proc. of ECCV 2016, 717–732.
- [6] Cadena, C., Carlone, L., Carrillo, H., Latif, Y., Scaramuzza, D., Neira, J., Reid, I., Leonard, J. J. Past, Present, and Future of Simultaneous Localization and Mapping: Toward the Robust-Perception Age. IEEE Trans. on Robotics 32 (6), 1309–1332. 2016.
- [7] Cimpoi, M., Maji, S., Kokkinos, I., Mohamed, S., Vedaldi, A. Describing Textures in the Wild. In Proc. of CVPR 2014, 3606–3613.
- [8] DeGol, J., Bretl, T., Hoiem, D. ChromaTag: A Colored Marker and Fast Detection Algorithm. In Proc. of ICCV 2017, 1472–1481.
- [9] Dogan, M. D., Garcia-Martin, R., Haertel, P. W., O’Keefe, J. J., Taka, A., Aurora, A., Sanchez-Reillo, R., Mueller, S. BrightMarker: 3D Printed Fluorescent Markers for Object Tracking. In Proc. of UIST 2023, 1–13.
- [10] Fiala, M. A Fiducial Marker System Using Digital Techniques. In Proc. of CVPR 2005, 590–596.
- [11] Gatrell, L. B., Hoff, W. A., Sklair, C. Robust Image Features: Concentric Contrasting Circles and Their Image Extraction. In Proc. of SPIE 1612, 235–245.
- [12] Gramazio, F., Kohler, M., d’Andrea, R. Flight Assembled Architecture. Editions HYX. 2012.
- [13] Grinchuk, O., Lebedev, V., Lempitsky, V. Learnable Visual Markers. In Proc. of NeurIPS 2016, 4150–4158.
- [14] Hawkins, T., Cohen, J., Debevec, P. A Photometric Approach to Digitizing Cultural Artifacts. In Proc. of VAST 2001, 333–342.
- [15] He, K., Zhang, X., Ren, S., Sun, J. Deep Residual Learning for Image Recognition. In Proc. of CVPR 2016, 770–778.
- [16] Herling, J., Broll, W. Advanced Self-Contained Object Removal for Realizing Real-Time Diminished Reality in Unconstrained Environments. In Proc. of ISMAR 2010, 207–212.
- [17] Hu, D., DeTone, D., Chauhan, V., Spivak, I., Malisiewicz, T. Deep ChArUco: Dark ChArUco Marker Pose Estimation. In Proc. of CVPR 2019, 8428–8436.
- [18] Jaderberg, M., Simonyan, K., Zisserman, A., Kavukcuoglu, K. Spatial Transformer Networks. In Proc. of NeurIPS 2015, 2017–2025.
- [19] Jia, J., Gao, Z., Zhu, D., Min, X., Zhai, G., Yang, X. Learning Invisible Markers for Hidden Codes in Offline-to-Online Photography. In Proc. of CVPR 2022, 2273–2282.
- [20] Jordà, S., Geiger, G., Alonso, M., Kaltenbrunner, M. The reacTable: Exploring the Synergy between Live Music Performance and Tabletop Tangible Interfaces. In Proc. of TEI 2007, 139–146.

[21] Kingma, D. P. and Ba, J. Adam: A Method for Stochastic Optimization. In Proc. of ICLR 2015, 1–15.

[22] Li, D., Nair, A. S., Nayar, S. K., Zheng, C. AirCode: Unobtrusive Physical Tags for Digital Fabrication. In Proc. of UIST 2017, 449–460.

[23] Lin, T., Maire, M., Belongie, S., Bourdev, L., Girshick, R., Hays, J., Perona, P., Ramanan, D., Zitnick, C. L., Dollár, P. Microsoft COCO: Common Objects in Context. In Proc. of ECCV 2014, 740–755.

[24] Liu, W., Anguelov, D., Erhan, D., Szegedy, C., Reed, S., Fu, C., Berg, A. C. SSD: Single Shot MultiBox Detector. In Proc. of ECCV 2016, 21–37.

[25] Lowe, D. Distinctive Image Features from Scale-Invariant Keypoints. *Intl. J. of Computer Vision* 60 (2), 91–110. 2004.

[26] Mann, S. Fung, J. EyeTap Devices for Augmented, Deliberately Diminished, or Otherwise Altered Visual Perception of Rigid Planar Patches of Real-World Scenes. *Presence* 11 (2), 158–175. 2002.

[27] Olson, E. AprilTag: A Robust and Flexible Visual Fiducial System. In Proc. of ICRA 2011, 3400–3407.

[28] Peace, J. B., Psota, E. T., Liu, Y., Pérez, L. E2ETag: An End-to-End Trainable Method for Generating and Detecting Fiducial Markers. In Proc. of BMVC 2020.

[29] Pintaric, T., Kaufmann, H. Affordable Infrared-Optical Pose-Tracking for Virtual and Augmented Reality. In Proc. of IEEE VR 2007 Workshop on Trends and Issues in Tracking for Virtual Environments, 44–51.

[30] Priyantha, N. B., Chakraborty, A., Balakrishnan, H. The Cricket Location-Support System. In Proc. of ACM MOBICOM 2000, 32–43.

[31] Redmon, J., Divvala, S., Girshick, R., Farhadi, A. You Only Look Once: Unified, Real-Time Object Detection. In Proc. of CVPR 2016, 779–788.

[32] Ren, S., He, K., Girshick, R., Sun, J. Faster R-CNN: Towards Real-Time Object Detection with Region Proposal Networks. *IEEE Trans. on Pattern Analysis and Machine Intelligence* 39 (6), 1137–1149. 2016.

[33] Romero-Ramirez, F. J., Muñoz-Salinas, R., Medina-Carnicer, R. Speeded Up Detection of Squared Fiducial Markers. *Image and Vision Computing* 76, 38–47. 2018.

[34] Ronneberger, O., Fischer, P., Brox, T. U-Net: Convolutional Networks for Biomedical Image Segmentation. In Proc. of MICCAI 2015, 234–241.

[35] Simonyan, K. and Zisserman, A. Very Deep Convolutional Networks for Large-Scale Image Recognition. In Proc. of ICLR 2015, 1–14.

[36] Takeuchi, Y. and Perlin, K. ClayVision: The (Elastic) Image of the City. In Proc. of CHI 2012, 2411–2420.

[37] Tancik, M., Mildenhall, B., Ng, R. StegaStamp: Invisible Hyperlinks in Physical Photographs. In Proc. of CVPR 2020, 2117–2126.

[38] Willis, K. D. D., Shiratori, T., Mahler, M. HideOut: Mobile Projector Interaction with Tangible Objects and Surfaces. In Proc. of TEI 2013, 331–338.

[39] Xu, M., Li, Q., Niu, J., Liu, X., Xu, W., Lv, P., Zhou, B. ART-UP: A Novel Method for Generating Scanning-Robust Aesthetic QR Codes. *ACM Trans. on Multimedia Computing, Communications and Applications* 17 (1), 1–23. 2021.

[40] Xu, M., Su, H., Li, Y., Li, X., Liao, J., Niu, J., Lv, P., Zhou, B. Stylized Aesthetic QR Code. *IEEE Transl on Multimedia* 21 (8), 1960–1970. 2019.

[41] Yaldiz, M. B., Meuleman, A., Jang, H., Ha, H., Kim, M. H. DeepFormableTag: End-to-end Generation and Recognition of Deformable Fiducial Markers. *ACM Trans. on Graphics* 40 (4), Article 67. 2021.

[42] Yang, Z., Bao, Y., Luo, C., Zhao, X., Zhu, S., Peng, C., Liu, Y., Wang, X. ARTcode: Preserve Art and Code In Any Image. In Proc. of UbiComp 2016, 904–915.

[43] Zhang, R., Isola, P., Efros, A. A., Shechtman, E., Wang, O. The Unreasonable Effectiveness of Deep Features as a Perceptual Metric. In Proc. of CVPR 2018, 586–595.

[44] Zhu, J., Kaplan, R., Johnson, J., Li, F. HiDDeN: Hiding Data with Deep Networks. In Proc. of ECCV 2018, 657–672.